International Journal of Mechanical Sciences 93 (2015) 22–31

Contents lists available at ScienceDirect

International Journal of Mechanical Sciences

journal homepage: www.elsevier.com/locate/ijmecsci

Modal method for dynamics analysis of cantilever type structures at large rotational deformations

Zhi-Peng Xue [a,b], Ming Li [a], Hong-Guang Jia [a,*]

[a] Changchun Institute of Optics, Fine Mechanics and Physics, Chinese Academy of Sciences, 3888, Dong Nanhu Road, Changchun 430033, China
[b] University of Chinese Academy of Sciences, 19, A Yuquan Road, Beijing 100049, China

ARTICLE INFO

Article history:
Received 28 April 2014
Received in revised form
12 November 2014
Accepted 3 January 2015
Available online 9 January 2015

Keywords:
Modal warping
Flexible multibody
Finite element
Leaf spring
Cantilever beam

ABSTRACT

The modal warping method is extended to a floating frame of reference formulation to combine modal warping formula with rigid body simulation. The highly nonlinear mass matrix because of the inertia coupling between the reference and the elastic displacements is approximated using the linear theory of elastodynamics. By kinematics analysis of infinitesimal deformation, the calculation of rotation deformations is derived. Then modal warping method is used to model deformations for numerical accuracy and computation efficiency. The rigid-flex multibody model for a leaf spring landing gear system is developed. The accuracy of the proposed method is examined by experimental/simulation comparison.

1. Introduction

Testing of dynamics behavior and control algorithms for an unmanned air vehicle (UAV) is difficult due to the delicate and expensive nature of UAV systems. Meanwhile field trial is very critical and high risk in autonomous UAV design. For these reasons the development life cycle of UAV system typically involves a period of simulation. Real-time simulation such as hardware in loop (HIL) simulation is often a component of virtual prototyping used to study the dynamics of UAV system prior to actual hardware development. HIL simulation can be used to test the UAV autopilot hardware reliability, test the closed loop performance of the overall system and tuning the control parameter [27,28]. However a real-time simulation may have difficulties in meeting real-time constraints for complex dynamics vehicle model simulations [29]. For the demand of enhancing the speed of real-time analysis, calculation time can be reduced by linearizing vehicle dynamics equations. It is also important to acknowledge the degree of accuracy lost when linearized equations are used [30,31]. Therefore a compromise between accuracy and speed should be reached in real-time simulation of UAV.

Developing a representative mathematical model involves quite a laborious process, especially for the landing gear system dynamics that is still an active research subject in the aircraft community. The landing gear can be modeled to different levels of details, ranging from a simple second order model for quantitative behavior to a sophsticated, modularized model to study the complex ground handling qualities with parametric analysis of the system [1,2]. In general the landing gear is regarded as an assembly of strut suspension with nonlinear suspension stiffness [3]. Collins [4] performed drop tests to study the damping of a landing gear system on a small aircraft that utilizes cantilever spring landing gear. Khapane [5] studied the gear walk instability by using flexible multibody dynamics simulation methods in SIMPACK.

However many small UAVs equipped with non-retractable landing gear use a cantilever beam system to provide stiffness to the gear, and these types of gear are popular due to their minimal weight and low aerodynamic drag. Since the leaf spring landing gear absorbs the impact kinetic energy by its elastic deformations, traditional modeling methods based on the type of shock absorber landing gear are not suitable for it. A lumped spring model is used based on an assumption that a multi-layered leaf spring can be modeled by a tapered beam [6]. This approach is too simple to take into account the effect of different deformation modes of the leaf spring in vehicle suspensions since all the spring characteristics are modeled by an equivalent spring constant. Rill et al. [7] divided leaf spring of a commercial vehicles into five rigid links connected to each other via rotational stiffnesses, and five links seem to be a reasonable compromise that achieve a fast simulated model but still captures the essential spring characteristics. They designed the leaf spring models as generalized force elements where the position, velocity and orientation of the axle mounting give the reaction forces in the chassis attachment positions.

Another approach used in modeling the leaf springs is based on using detailed finite element (FE) models that elastic component is

* Corresponding author. Tel.: +86 431 8670 8211; fax: +86 431 8617 8857.
E-mail addresses: xuezhipengss1314@126.com (Z.-P. Xue), jiahg@ciomp.ac.cn (H.-G. Jia).

http://dx.doi.org/10.1016/j.ijmecsci.2015.01.003
0020-7403/

approximated to a continuous set of degree of freedom (DOF) [8,9]. In order to reduce the number of DOF and, thus, to increase computational efficiency, a wide-spread method is modal analysis that vibrations mode shapes are used to replace the n-coupled differential equations with n-uncoupled equations, where each uncoupled equation represents the motion of the system for that mode of vibration [10]. In this technique, a body's deformation can be approximated by a linear superposition of pre-selected shape functions. Then, the problem of calculating the deformation is transformed to that of finding the weights of the modes and good approximate solutions can be obtained via superposition with only first few mode shapes. The primary advantage of this method is that, due to the orthogonal property of normal modes, the transformed equations decouple, provided that the equations for the physical system are linear. Another advantage of modal superposition is that generally the number of equations to predict the response of the structure with reasonable accuracy in modal space is significantly less than the number of equations that represent the physical system [11]. So the modal method has been a popular technique for the analysis of structures and real-time simulations [12,13].

However, the linear approximated modal method is based on a linear strain tensor and it does not account for rotational deformations. Some recommendations regarding the limits of this assumption are given by Mayo [14]. Meanwhile large displacement response of the leaf spring landing gear may be caused by a high impact velocity, and the magnitudes of its bending or twisting deformations are relatively large. Therefore the linear modal method can exhibit significant errors when applied to leaf spring modeling. Recent research has occurred to address the limitation of the linear method. For large deformations, many authors take the approach of partitioning the stiffness and damping matrices into linear and nonlinear parts, and the nonlinear parts are as a vector of pseudo-forces [15,16]. On the other hand, the effects of rotational deformation of some cantilever components e.g. leaf spring and wings cannot be ignored, for the deformation of these components may be subjected to small deformations but relative large rotations. Sugiyama et al. [17] developed a nonlinear elastic model of leaf springs for use in the computer simulation of multibody vehicle systems. The distributed inertia and stiffness of the leaves of the spring are modeled using the finite element floating frame of reference formulation that accounts for the effect of the nonlinear dynamic coupling between the finite rotations and the leaf deformation. Wang et al. [18] investigated a homotopy analysis method to calculate the large deformation of a cantilever beam under point load at the free tip. They also give explicit analytic formulas for the rotation angle at the free tip, which provide a convenient and straightforward approach to calculate the vertical and horizontal displacements of a cantilever beam with large deformation. Pai et al. [19] presented a total-Lagrangian displacement-based finite-element formulation for general anisotropic beams undergoing large displacements and rotations. To improve the computational efficiency, Müller et al. [20] proposed a stiffness warping method that is stable and fast like linear models, in the case of tetrahedral elements that track the rotation of each node and warps the stiffness matrix. Ngan et al. [21] extended the stiffness warping to more complex nonlinear elements, particularly hexahedra and quadratic tetrahedral.

The modal warping method [32] was introduced by Choi and Ko, and it is an approach to eliminate the linearization artifacts while retaining the efficiency of modal analysis. The basic idea of the modal warping approach is to embed a local coordinate frame at each simulation node, and tracks the local rotations that occur during the deformation based on the infinitesimal rotation tensor, and warps the pre-computed modal basis in accordance with the local rotations of the mesh nodes. Guo and Qin [33] exploited modal warping technique into their meshless simulation framework to achieve real-time manipulation and deformation. However typical applications for above approaches are generally in graphics computers such as virtual surgery, virtual sculpting, video games, etc. To demonstrate the advantages of the approach, researchers also compared it to a linear and a non-linear model through numerical simulation [20,32]. While further comparison between experimental data and numerical results are required to show that results from theory correlate well to experiment before the modal warping approach is implemented into real-world systems such as a land gear system or a UAV multibody system.

Choi and Ko's work [32] focuses primarily on extending the modal warping method to cope with manipulation constraints for simulating constrained deformable objects attached to rigid supports which is motivated by the work of Hauser et al. [13]. This paper is a contribution to extend the modal warping method to a floating frame of reference formulation (FFRF) to model a deformable body undergoes both large rigid body motion and small deformations which can be used for a real-time simulation. The objective of this work is to model a leaf spring landing gear system for dynamics analysis. Another objective of this study is to investigate the potential of the proposed approach to be used in UAV multibody system modeling for HIL simulations in the future. The accuracy and computational speed of the proposed method are also acknowledged in this study. Based on this model, a rigid-flex multibody model for the real-time simulation of a UAV system with a leaf spring landing gear can be further developed. The focus holds on the following aspects:

- A detailed description of the calculation of rotational deformation is given to show how rotational part of deformations can be easily and effectively obtained.
- Describe how to extend the modal warping method to a multibody system based on FFRF, and linear theory of elastodynamics is used to reduce calculation time.
- Show that a simplified flexible multibody with deformations computed using the modal warping method can offer significant accuracy and efficiency advantages.

In the next section a brief overview of a general modal method is summarized. More details are available in [22]. In Section 3, kinematics of infinitesimal deformation is investigated firstly to obtain the rotation matrix for every vertex. Then in order to integrate the rotational deformations, a local coordinate frame is embedded which is used to measure the local rotations with respect to the global coordinate frame. Section 4 introduces a simplified flexible multibody dynamics that the highly nonlinear of the mass matrix caused by the limited rotation of the deformation is approximated using the linear theory of elastodynamics. Section 5 presents numerical examples and experiments followed by conclusions in Section 6.

2. Modal theory

2.1. Modal superposition

The necessary background on modal vibration analysis is briefly summarized here. The modal analysis of a physical system begins with a linear set of equations that describe the system's behavior. The elastodynamic equations for a finite element model have a general form:

$$M\ddot{u}+C\dot{u}+Ku=f \tag{1}$$

where M, C, and K are respectively known as the system's stiffness, damping, and mass matrices, u and f respectively are the vector of generalized displacements and forces. The displacement vector u is then expanded in a modal displacement basis,

$$u(t)=\Phi\eta(t) \tag{2}$$

where Φ denotes the modal matrix, a matrix whose ith column Φ_i represents the ith mode shape, and $\eta(t)$ is the vector of modal coordinates. An important property is that the modal matrix Φ is

independent of time, and completely characterized by values at mesh vertices.

Substituting Eq. (2) into (1) and premultiplying by Φ^T,

$$M_\eta \ddot{\eta} + C_\eta \dot{\eta} + K_\eta \eta = Q \tag{3}$$

in which

$$M_\eta = \Phi^T M \Phi = I \tag{4}$$

$$K_\eta = \Phi^T K \Phi = \mathrm{diag}(w_i^2) \tag{5}$$

$$C_\eta = \Phi^T C \Phi \tag{6}$$

$$Q = \Phi^T f \tag{7}$$

where M_η denotes an identity matrix and K_η is a diagonal matrix that contains in its ith column the squared eigen frequency ω_i corresponding to mode number i.

The damping matrix is defined as a linear combination of M and K according to the Rayleigh form:

$$C = \alpha M + \beta K \tag{8}$$

where α is mass proportional Rayleigh damping coefficient, β is the stiffness proportional Rayleigh damping coefficient. We know that M and K are diagonalized by operating on them with the modal matrix. When C is a linear combination of M and K, then the damping matrix C is also diagonalized by the same pre- and post-multiplication operations by the modal matrix as with the M and K matrices

$$C_\eta = \alpha I + \beta K_q \tag{9}$$

Define the critical damping $C_{cr} = 2\sqrt{KM}$ [10] and rewrite C_η as

$$C_{\eta i} = \alpha + \beta \omega_i^2 = 2\xi_i \omega_i \tag{10}$$

where ξ_i is the percentage of critical damping for the ith mode, defined as

$$\xi_i = \left(\frac{C_i}{C_{cr}}\right)_i = \frac{C_i}{2\sqrt{K_i M_i}} \tag{11}$$

Then,

$$\xi_i = \frac{\alpha + \beta \omega_i^2}{2\omega_i} \tag{12}$$

This type of damping is known as proportional damping, where the damping for each mode is proportional to the critical damping for that mode. For lightly damped systems, proportional damping can be added, while still allowing the equations to be uncoupled. Then Eq. (3) is transformed into a set of single DOF equations in modal space:

$$\ddot{\eta}_i + 2\xi_i \omega_i \dot{\eta}_i + \omega_i^2 \eta_i = Q_i \tag{13}$$

The set of single DOF corresponding to individual modes can be compute independently and combined by linear superposition using Eq. (2).

2.2. Modal reduction

A specific characteristic of the FE model is a very high number of nodes n. Since each node has 3 translational DOFs, the system dimension is $3n$. In order to reduce this high number, we can discard modes that will have no significant effect on the deformation. Removing modes that are too stiff and too high frequency to be observed will not change the appearance of the resulting simulation, but removing them will greatly reduce the simulation's cost [23].

Then the next step in creating the elastic model is to sort vibration modes so that only the most important modes are kept. Frequency response analysis is used to determine the contributions of each mode to the deformation. Generally the model of elastic deformation is a multiple input multiple output (MIMO) model. The desired magnitude can be extracted as Z_i/F_j, where Z_i is the DOF whose displacement is desired and F_j is the DOF where the force is applied [10].

3. Modeling deformation

In this section the kinematics of infinitesimal deformation is commenced to show how such deformations can be decomposed into a strain and a rotation. Then this decomposition is used to extend modal analysis so that it keeps track of rotations, while still retaining the basic framework of modal analysis.

3.1. Kinematics of infinitesimal deformation

As shown in Fig. 1, vector x denotes the position of point P_0 in the undeformed state, which moves to a new position $a(x)$ due to a displacement vector $u(x)$. The position of P in the deformed state is

$$a(x) = x + u(x) \tag{14}$$

Differentiating both side of the above equation with respect to x as

$$da = (I + \nabla u)dx \tag{15}$$

Where ∇u is the gradient of the displacement vector, and ∇ is written as

$$\nabla = \frac{\partial}{\partial x_1}\mathbf{i} + \frac{\partial}{\partial x_2}\mathbf{j} + \frac{\partial}{\partial x_3}\mathbf{k} \tag{16}$$

Since both $u(x)$ and x are first-order tensor, the gradient of the displacement vector ∇u is a second-order tensor and can be written as

$$\nabla u = \begin{bmatrix} \varepsilon_{11} & \varepsilon_{12} & \varepsilon_{13} \\ \varepsilon_{21} & \varepsilon_{22} & \varepsilon_{23} \\ \varepsilon_{31} & \varepsilon_{32} & \varepsilon_{33} \end{bmatrix} \tag{17}$$

in which

$$\varepsilon_{ij} = \frac{\partial u_i}{\partial x_j} \tag{18}$$

where $1 \le i \le 3$, $1 \le j \le 3$, generally $\varepsilon_{ij} \ne \varepsilon_{ji}$, so the gradient of the displacement ∇u is not symmetric. Since ∇u is a second-order tensor, it can be represented as the sum of a symmetric and

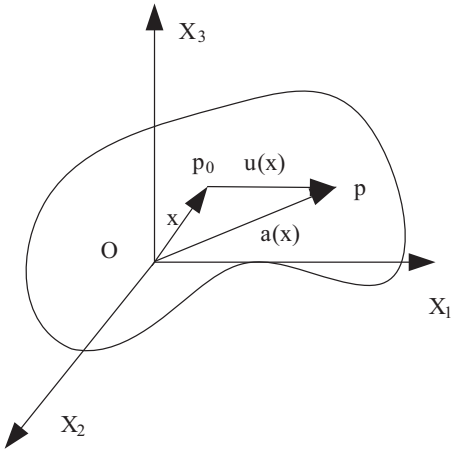

Fig. 1. Kinematics of infinitesimal deformation.

antisymmetric tensor, that is

$$\nabla u = \varepsilon + \omega \tag{19}$$

where

$$\varepsilon = \frac{1}{2}(\nabla u + \nabla u^T) = \begin{bmatrix} e_{11} & e_{12} & e_{13} \\ e_{21} & e_{22} & e_{23} \\ e_{31} & e_{32} & e_{33} \end{bmatrix} \tag{20}$$

$$\omega = \frac{1}{2}(\nabla u - \nabla u^T) = \begin{bmatrix} 0 & \omega_{12} & \omega_{13} \\ \omega_{21} & 0 & \omega_{23} \\ \omega_{31} & \omega_{32} & 0 \end{bmatrix} \tag{21}$$

in which $2e_{ij} = 2e_{ji} = \varepsilon_{ij} + \varepsilon_{ji}$, $2\omega_{ij} = \varepsilon_{ij} - \varepsilon_{ji} = -2\omega_{ji}$, ε is the infinitesimal strain tensor, which measures the change in the squared length of dx during an infinitesimal deformation, and ω is the infinitesimal rotation tensor, which measures the mean rotation of a volume element.

The rotation vector w is defined as

$$w = \frac{1}{2}\nabla \times u \tag{22}$$

Then the skew-symmetric tensor ω can be written as

$$\omega = \frac{1}{2}(\nabla u - \nabla u^T) = \frac{1}{2}(\nabla \times u) \times = w\times \tag{23}$$

where $w\times$ denotes the standard skew symmetric matrix of vector w.

By substituting Eq. (19) and (23) into (15), we obtain

$$da = dx + \varepsilon dx + w \times dx \tag{24}$$

which shows that an infinitesimal deformation consists of a strain and a rotation, and the rotational part can be extracted by calculating the curl of the displacement as Eq. (22).

3.2. Rotational deformation of finite element

In this section the rotation vector $w(t)$ will be represented in modal coordinates, and the effect of it is integrated into the calculation of the displacement field $u(t)$.

3.2.1. Rotation vector of finite element

Finite element modeling involves decomposing a body into a set of discrete volumetric elements, each associated with a set of boundary nodes and shape functions that interpolate a quantity within the element from the quantity's nodal values. The displacement of an arbitrary node in element e can be approximated as

$$u(x) = N_e(x)u_e \tag{25}$$

where $u_e = [u_{e,1}^T | \ldots | u_{e,k}^T]$ is the vertex displacement of element e, and k is the number of vertex nodes in the element. $N_e(x)$ is the linear shape function of the element. Substituting Eq. (25) into Eq. (22) yields the rotation vector of element e

$$w_e(x) = \frac{1}{2}(\nabla \times)N_e(x)u_e = W_e u_e \tag{26}$$

Note that because $N_e(x)$ is a linear function of x, W_e is constant. For the rotation vector of a node, the average of the rotation vectors of all the elements sharing the node is used. Let W be the global matrix that contains W_e of all the elements, and expanding u_e with Eq. (2) gives

$$w(t) = Wu(t) = W\Phi\eta(t) = \Psi\eta(t) \tag{27}$$

Equation above provides an efficient way to represent the rotation vector $w(t)$ at each node in terms of $\eta(t)$. Both W and Φ are constant over time; therefore the modal rotation matrix Ψ can be precomputed.

3.2.2. Building matrix W

As Eq. (26) shows the Matrix W can be written as

$$W = \frac{1}{2}(\nabla \times)N(x) \tag{28}$$

For simplicity, linear tetrahedral elements are used. $u_e = [u_{e,1}^T | u_{e,2}^T | u_{e,3}^T | u_{e,4}^T]$ is the vertex displacement of element e, in which the displacement of vertex i is $u_{e,i}^T = [x_{ei}, y_{ei}, z_{ei}]^T$. The shape function $N_e(x)$ can be written as

$$N_e = \begin{bmatrix} N_1 & 0 & 0 & N_2 & 0 & 0 & N_3 & 0 & 0 & N_4 & 0 & 0 \\ 0 & N_1 & 0 & 0 & N_2 & 0 & 0 & N_3 & 0 & 0 & N_4 & 0 \\ 0 & 0 & N_1 & 0 & 0 & N_2 & 0 & 0 & N_3 & 0 & 0 & N_4 \end{bmatrix} \tag{29}$$

where N_i is the linear function of the vertex node i.

A tetrahedral element is shown in Fig. 2, and a point P inside it divides the tetrahedron in four sub-tetrahedrons. The tetrahedral barycentric coordinates of the point P are given by

$$L_1 = \frac{V_{P234}}{V_{1234}}, L_2 = \frac{V_{P134}}{V_{1234}}, L_3 = \frac{V_{P124}}{V_{1234}}, L_4 = \frac{V_{P123}}{V_{1234}} \tag{30}$$

where V_{ijkl} is the volume of the tetrahedron with vertices at i, j, k and l. Hence, the coordinates of vertex 1 are (1,0,0,0), those of vertex 2 are (0,1,0,0), etc. The transformation from physical to tetrahedral coordinates is

$$\begin{Bmatrix} 1 \\ x \\ y \\ z \end{Bmatrix} = \begin{bmatrix} 1 & 1 & 1 & 1 \\ x_1 & x_2 & x_3 & x_4 \\ y_1 & y_2 & y_3 & y_4 \\ z_1 & z_2 & z_3 & z_4 \end{bmatrix} \begin{Bmatrix} L_1 \\ L_2 \\ L_3 \\ L_4 \end{Bmatrix} \tag{31}$$

where the coordinates x_i, y_i, z_i correspond to the vertex i. Therefore, the tetrahedral barycentric coordinates can be written as

$$\begin{Bmatrix} L_1 \\ L_2 \\ L_3 \\ L_4 \end{Bmatrix} = \frac{1}{6V_{1234}} \begin{bmatrix} a_1 & b_1 & c_1 & d_1 \\ a_2 & b_2 & c_2 & d_2 \\ a_3 & b_3 & c_3 & d_3 \\ a_4 & b_4 & c_4 & d_4 \end{bmatrix} \begin{Bmatrix} 1 \\ x \\ y \\ z \end{Bmatrix} \tag{32}$$

in which

$$a_i = \det \begin{bmatrix} x_j & y_j & z_j \\ x_k & y_k & z_k \\ x_l & y_l & z_l \end{bmatrix}, \quad b_i = -\det \begin{bmatrix} 1 & y_j & z_j \\ 1 & y_k & z_k \\ 1 & y_l & z_l \end{bmatrix}$$

$$c_i = -\det \begin{bmatrix} y_j & 1 & z_j \\ y_k & 1 & z_k \\ y_l & 1 & z_l \end{bmatrix}, \quad d_i = -\det \begin{bmatrix} y_j & z_j & 1 \\ y_k & z_k & 1 \\ y_l & z_l & 1 \end{bmatrix} \tag{33}$$

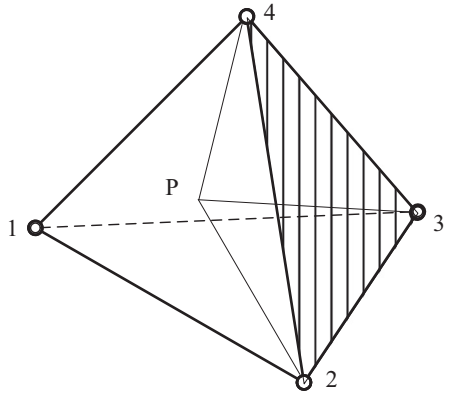

Fig. 2. Tetrahedral element.

In Eq. (32) the linear function is represented in terms of tetrahedral coordinates, which means that $N_i = L_i$, then the matrix W for node i can be written as

$$W_i = \frac{1}{2}(\nabla\times)N_i(x) = \frac{1}{2}\begin{bmatrix} 0 & -\frac{\partial}{\partial z} & \frac{\partial}{\partial y} \\ \frac{\partial}{\partial z} & 0 & -\frac{\partial}{\partial x} \\ -\frac{\partial}{\partial y} & \frac{\partial}{\partial x} & 0 \end{bmatrix}\begin{bmatrix} L_i & & \\ & L_i & \\ & & L_i \end{bmatrix} \tag{34}$$

Assembling the matrix W_e of element e as

$$W_e = [W_1, W_2, W_3, W_4] \tag{35}$$

3.3. Modal warping implementation

In sections above, a brief approach to compute the rotation of deformation is given. To further integrate the effect of the rotational part into the calculation of displacement, a local coordinate frame is embed to measure the local rotations with respect to the global coordinate frame as shown in Fig. 3. The displacement vector u_i in Eq. (1) represents the displacement of vertex i from its original position, measured in the global coordinate frame, and u_i^L is defined as the displacement of vertex i, measured in the local coordinate at node i. Let $D_i(t)$ be the rotation matrix representing the orientation of local coordinate at node i. Then the displacement vector u can be written as

$$u(t) = D(t)u^L(t) = D(t)\Phi\eta^L(t) \tag{36}$$

where $\eta^L(t)$ is the vector of local modal coordinates. Instead of solving Eq. (3) for u, we can convert the equation into local coordinate that can be solved for u^L. Based on the modal warping method [32] Eq. (3) is rotated to local coordinate using the inverse D^{-1}. The local modal displacements are then computed in this local coordinates and then rotate back to global coordinates using D. Therefore Eq. (3) in local modal coordinates can be written as

$$M_q\ddot{\eta}^L + C_q\dot{\eta}^L + K_q\eta^L = \Phi^T D^{-1} f \tag{37}$$

in which

$$D = \left[I + \tilde{\nu}\ \sin\ \theta + 2\tilde{\nu}^2 sin^2\frac{\theta}{2}\right] \tag{38}$$

Rodrigues' formula is used to convert the rotation vector $w(t)$ of each node into the rotation matrix. It expresses the rotation matrix in terms of the angle $\theta = \|w(t)\|$ and the unit axis $\nu = w(t)/\|w(t)\|$ of rotation.

4. Simplified flexible multibody dynamics

4.1. System equations of motion

The most frequently used approach in multibody simulation to consider body flexibility is the FFRF as demonstrated [24–26]. The configuration of each deformable body in the multibody system is identified by using two sets of coordinates: reference and elastic coordinates. Reference coordinates define the location and orientation of a selected body reference. Elastic coordinates, on the other hand, describe the body deformation with respect to the body reference. The global position of an arbitrary point B on the deformable body i is thus defined as

$$r_i^B = r_i + A_i(x^B + u^B) \tag{39}$$

where r_i is the position vector of the origin body reference, A_i is the transformation matrix, x^B is the position vector of the point B in undeformed state, and u^B is the vector of elastic coordinates which can be represented by Eq. (36). Thus, we can define the coordinates of body i as

$$q^i = \begin{bmatrix} R^i \\ \theta^i \\ q_f^i \end{bmatrix} \tag{40}$$

where R^i and θ^i are the reference coordinates and q_f^i is the elastic coordinates.

The equations of motion of Lagrangian formalism in multibody systems have been proposed in [24]. It will not be reviewed in the present paper. The final form of the equations of motion expressed in generalized coordinates is

$$\begin{bmatrix} m_{RR}^i & m_{R\theta}^i & m_{Rf}^i \\ & m_{\theta\theta}^i & m_{\theta f}^i \\ \text{symmetric} & & m_{ff}^i \end{bmatrix}\begin{bmatrix} \ddot{R}^i \\ \ddot{\theta}^i \\ \ddot{q}_f^i \end{bmatrix} + \begin{bmatrix} 0 & 0 & 0 \\ 0 & 0 & 0 \\ 0 & 0 & K_{ff}^i \end{bmatrix}\begin{bmatrix} R^i \\ \theta^i \\ q_f^i \end{bmatrix} + \begin{bmatrix} C_{R^i}^T \\ C_{\theta^i}^T \\ C_{q_f^i}^T \end{bmatrix}$$

$$\lambda = \begin{bmatrix} (Q_e^i)_R \\ (Q_e^i)_\theta \\ (Q_e^i)_f \end{bmatrix} + \begin{bmatrix} (Q_v^i)_R \\ (Q_v^i)_\theta \\ (Q_v^i)_f \end{bmatrix} \tag{41}$$

under the constraints

$$C(R,\ \theta,\ q_f) = 0 \tag{42}$$

where m_{ij} represents mass submatrices, K_{ff} is the stiffness matrix, λ is the vector of Lagrange multiplier, matrix C^T represents the

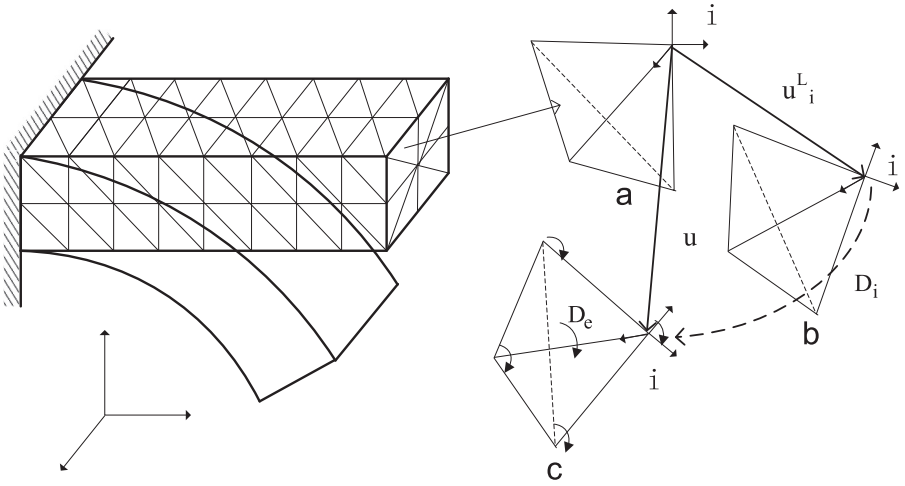

Fig. 3. Deformation of cantilever with the rotation of local coordinates frames.

transposition of the constraint Jacobian matrix, Q_e is the vector of external force and Q_v is the vector of quadratic velocity.

4.2. Linear theory of elastodynamics

To introduce the dynamics formulation based on the linear theory of elastodynamics, we rewrite Eq. (41) in the following partitioned form:

$$\begin{bmatrix} m_{rr}^i & m_{rf}^i \\ m_{fr}^i & m_{ff}^i \end{bmatrix} \begin{bmatrix} \ddot{q}_r^i \\ \ddot{q}_f^i \end{bmatrix} + \begin{bmatrix} 0 & 0 \\ 0 & K_{ff}^i \end{bmatrix} \begin{bmatrix} q_r^i \\ q_f^i \end{bmatrix} = \begin{bmatrix} \overline{Q}_r^i \\ \overline{Q}_f^i \end{bmatrix} \tag{43}$$

where $q_r^i = \left[R^{iT}\ \theta^{iT}\right]^T$ is the vector of reference coordinates of body i; $\overline{Q}^i$ is the vector of generalized forces, including the external forces, reaction forces, and the quadratic velocity force as

$$\overline{Q}^i = Q_e^i + Q_v^i - C_{qi}^T \lambda \tag{44}$$

Rigid body motion and flexible deformation interact with each other though inertial effects. The mixed set of reference and elastic coordinates of deformable body leads to a highly nonlinear mass matrix as a result of the inertia coupling between the reference and the elastic displacements, and the mass matrix must be iteratively updated. The deformation body is rotating rapidly, neither these effects will be significant. Therefore to increase computational efficiency, a solution strategy that has been used in the past to treat the multibody system first as rigid body systems as Eq. (45). In this assumption, the effect of the elastic deformation on rigid body motion is ignored. Then the term $m_{rf}^i \ddot{q}_f^i$ in Eq. (43) is neglected as

$$\begin{bmatrix} m_{RR}^i & \\ & m_{\theta\theta}^i \end{bmatrix} \begin{bmatrix} \ddot{R}^i \\ \ddot{\theta}^i \end{bmatrix} + \begin{bmatrix} C_{R^i}^T \\ C_{\theta^i}^T \end{bmatrix} \lambda = \begin{bmatrix} (Q_e^i)_R \\ (Q_e^i)_\theta \end{bmatrix} + \begin{bmatrix} (Q_v^i)_R \\ (Q_v^i)_\theta \end{bmatrix} \tag{45}$$

Eq. (45) can be solved for the inertia and reaction force by general multi-rigid-body computer programs. These forces are then introduced to the elastic deformable model as Eq. (46) to solve for the deformation displacements. The total motion of a deformable body is then obtained by superimposing the small elastic deformation on the gross rigid body motion.

$$m_{ff}^i \ddot{q}_f^i + K_{ff}^i q_f^i = \overline{Q}_f^i - m_{fr}^i \ddot{q}_r^i \tag{46}$$

Rewrite Eq. (46) in modal coordinates based on modal warping formula, we have

$$M_\eta \ddot{\eta}^L + C_\eta \dot{\eta}^L + K_\eta \eta^L = \Phi^T D^{-1} (\overline{Q}_f^i - m_{fr}^i \ddot{q}_r^i) \tag{47}$$

Then the simplified flexible multibody dynamics can be accomplished by combing the modal warping method with a standard rigid-body dynamics program. The modal warping formula is embedded in a rigid-body reference frame, and both systems evolve over time.

4.3. Algorithm

Summarize the entire flexible multibody simulation algorithm

1. Precomputed
   - Modal datum: eigenvalues and eigenvectors
   - Assembling matrix W
   - Modal rotation matrix Ψ
   - Rigid body system parameters
2. Loop
   - Rigid body simulation solve:
     Inertia and reaction force, rigid body motion
   - Elastic deformation solve (modal warping method):
     Deformation displacements
   - Deformable body motion:
     Superimpose deformation on rigid body motion

5. Application cases

In this section, a simple cantilever beam and a drop system are chosen to show the effectiveness of the proposed method. The eigenvalues and the corresponding eigenvectors are calculated by finite element analysis program Nastran.

5.1. Cantilever beam

This experiment is to compare the results generated by the linear modal method, modal warping method and nonlinear FEM. The dimensions of the beams are 40 mm in width, 20 mm in thickness and 200 mm in length, with a load force at the tip. The parameters of the structure are: a density of 2700 kg/m^3 and a Young modulus of 70×10^6 Pa. Its FE model has 82 nodes and 196 tetrahedral elements. The beam is assumed to be straight and undeformed in its initial configuration. Fig. 4 shows several linear and warped mode shapes respectively.

The three methods indicated previously are used respectively to deform the cantilever under different forces. The nonlinear FE analysis is implemented in program Nastran, and the results of it are taken to compare with the other two methods. Table 1 shows the vertical displacements of the tip node by the three methods.

Results obtained by nonlinear FEM are as the ground truth, and the relative vertical displacement errors are shown in Fig. 5. Comparison with the linear method shows that the proposed modal warping method really improves the accuracy of deformations. Note that the relative errors in both methods increases as the forces/deformations increases, and the error of warping model with 4000 N case is only 10%, while the error of linear model is larger than 40% in this case. Fig. 6 shows the snapshots taken at the equilibrium states of the cantilever, which shows the relative volume change with respect to the initial volume. A large relative volume error can be observed in the linear model as the load force increases, while it was not easy to visually discriminate between the results produced by modal warping and nonlinear FEM, unless the load force is bigger than 2500 N. It can be found in Figs. 5 and 6 that the numerical res-

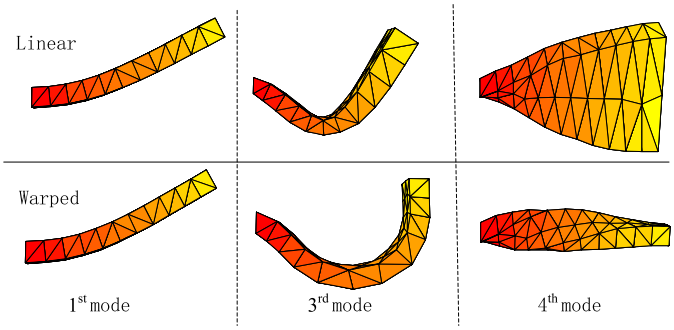

Fig. 4. Linear and warped mode shapes of cantilever.

Table 1
Vertical displacements at tip node (mm).

Method	Load force(N)							
	500	1000	1500	2000	2500	3000	3500	4000
Linear	22.20	44.40	66.60	88.79	110.99	133.16	155.39	177.59
Warped	22.24	44.15	65.04	84.40	101.63	116.27	127.88	136.13
Nonlinear	22.43	44.12	63.73	80.61	94.74	106.43	116.11	124.15

ults obtained by the modal warping method show a good agreement with the results given by nonlinear FEM.

5.2. Main landing gear

The cantilever simulations have shown a high accuracy of the modal warping in statics analysis. This section will demonstrate its stability and manipulation capability in dynamics analysis. Leaf spring landing gear is made with layers of different composite materials. Its FE model has 471 nodes and 1110 tetrahedral elements. The first 6 modes are rigid body modes resulting from a free-free modal analysis. Table 2 shows the 7th to 18th modes.

We define the vertical direction is the *Z* direction and *Y* direction is corresponding to the lateral direction. Fig. 7 shows respectively, the frequency response for vertical displacement (Z–Z) and lateral displacement (Z–Y) due to a unit vertical force at the node connected the leaf spring with the wheel, using the first 50 modes except the rigid modes. The contributions of modes decrease as their frequencies increase. Note that the amplitude values for 13th and 17th mode are almost same. The modes which are eliminated have low magnitude relative to the 17th mode. Therefore we use 11 vibration modes from 7th to 17th to construct the flexible model of leaf spring. Fig. 8 shows exemplarily selected mode shapes of the leaf spring. Modes 7, 10, 11 and 17 are modes which involve motion only in the Y–Z plane, bending type motions.

5.2.1. Statics experiments

Fig. 9 shows the statics experiment setup of the leaf spring. The leaf spring is mounted on a test bench with a load mass at the tip. The results of it are taken to compare with the two modal methods. In Table 3 the vertical displacements of simulation results and experimental records at the measuring point for different load masses are presented.

Table 2
Modal results of leaf spring (rad/s).

Modes	Frequency	Modes	Frequency
7	107	13	1927
8	322	14	2945
9	494	15	3393
10	641	16	3453
11	1261	17	3849
12	1294	18	4234

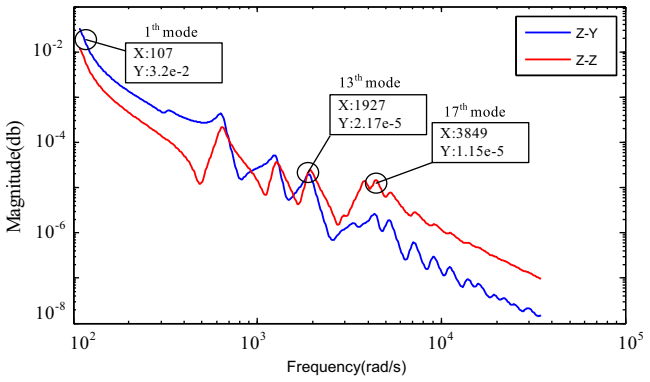

Fig. 7. Frequency response analysis of leaf spring.

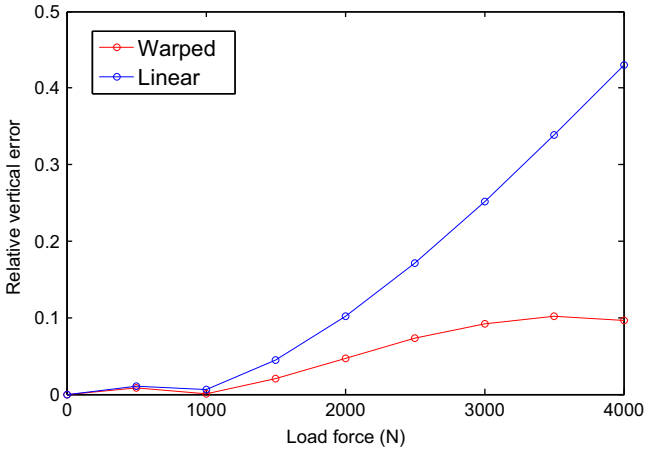

Fig. 5. Error analysis of the displacements shown in Table 1.

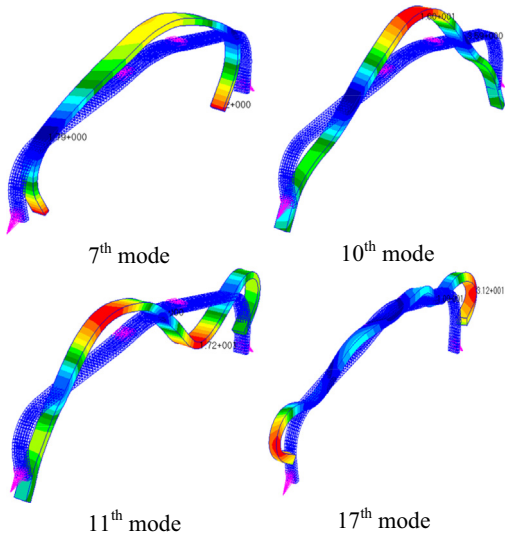

Fig. 8. Mode shapes of leaf spring.

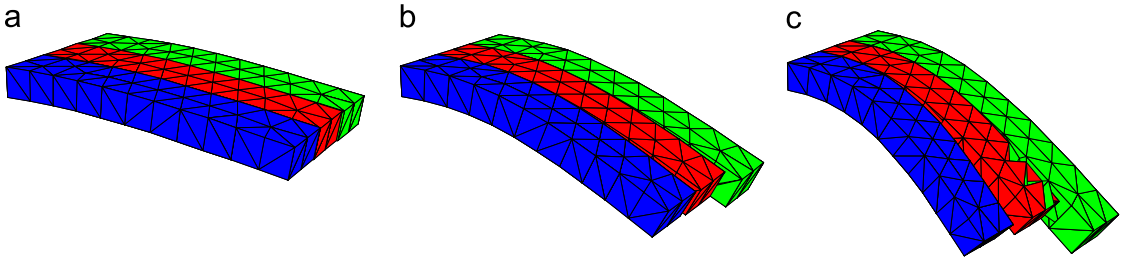

Fig. 6. Cantilever deformed by the linear modal (green), by modal warping (red), and by nonlinear FEM (blue) under different load forces. (For interpretation of the references to color in this figure legend, the reader is referred to the web version of this article.)

The relative vertical and lateral displacement errors are shown in Fig. 10. A load mass of 100 kg is the design landing mass at each gear, and the relative errors are below 5% for both the linear modal and modal warping method; therefore the accuracy for two methods is very good when the load mass is less than 100 kg. The error on the displacement increases with the increasing load mass. Even though the load has reached to 180 kg which represents the maximum realistic condition for landing, the error of the modal warping method remains within 10%, while the error of linear modal has been more than 35%.

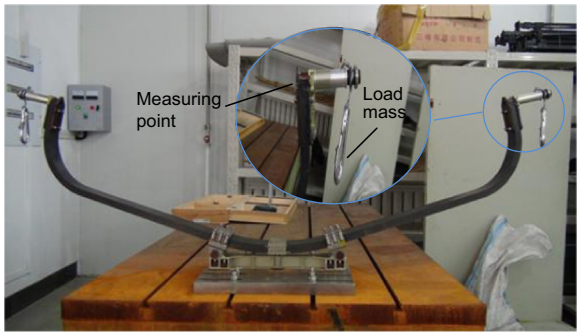

Fig. 9. Statics experiment setup of leaf spring.

Table 3
Vertical displacements at measuring point (mm).

Method	Load force(*N*)							
	20	40	60	80	100	120	140	180
Linear	10.16	20.33	30.48	40.64	50.80	60.96	71.13	91.44
Warped	10.08	20.84	30.36	39.60	49.11	56.83	65.00	73.57
Experiment	10.26	21.02	30.06	39.14	48.56	55.12	61.48	67.24

5.2.2. *Drop experiments*

The drop system as shown in Fig. 11 basically consists of four parts: a landing gear, a pair of wheels, a load mass and measuring unit. A drop test is performed to simulate actual landing loads experienced from a 1.8 m/s impact with the landing mass 100 kg. The drop mass is attached to the top of the landing gear. Initially, all the wheels are at rest. Video footage is used to capture the vertical and lateral displacements. Fig. 12 shows the frames of video footage when wheels are undergoing, respectively, fully compressed, maximum rebound and stationary state. Freedom of lateral movement to the gear legs is given so that lateral stiffness or damping would not be influenced by other motion-induced stiffness components.

The flexible multibody dynamics with deformation computed using modal warping method (warping-multibody) is carried out by using the Matlab/Simulink program and SimMechanics library is used to model the rigid-body system. The heights of the landing gear's center of gravity (CG) for both experimental records and the simulation are shown in Fig. 13. The heights of experimental records are taken from the frames of video footage for every 50 ms. The simplified flexible multibody analysis highlights a good agreement between the drop experimental data and simulation results. It is, however, very difficult, if not impossible, to tune the damping in such a way that it perfectly corresponds for the drop test.

For comparison we also implement a drop simulation with deformation computed using linear method (linear-multibody). Fig. 14 shows the experimental records and the simulation results when the landing gear undergoes fully compressed. The difference between the

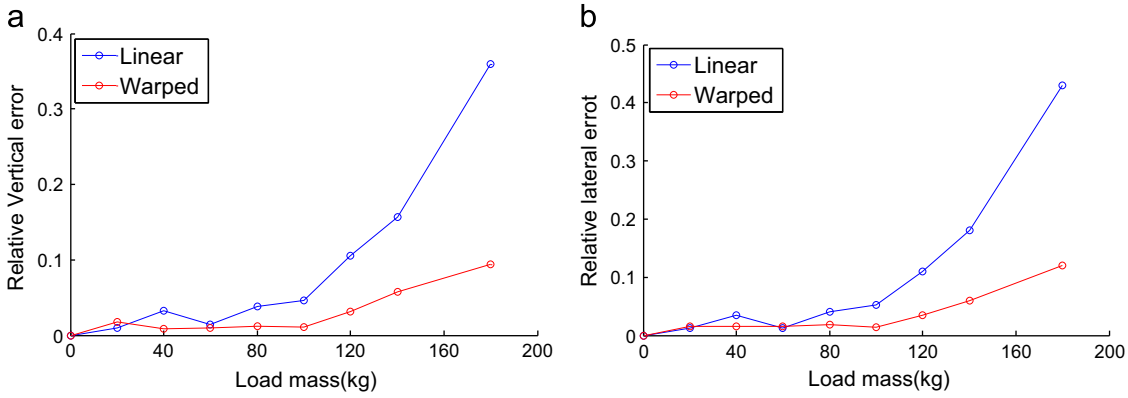

Fig. 10. Displacement errors of the leaf spring in static analysis. (a). Vertical errors (b). Lateral errors.

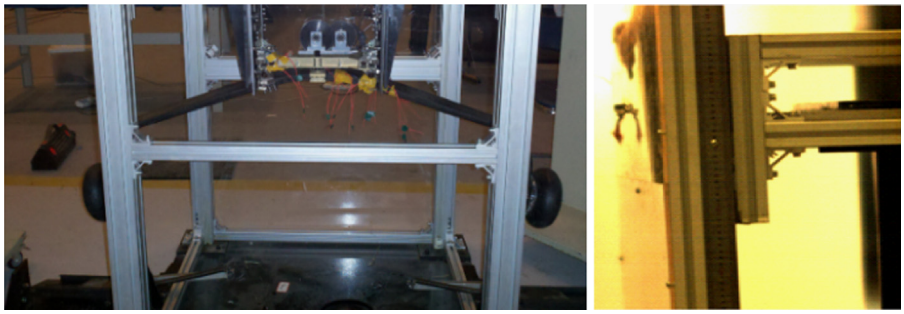

Fig. 11. Drop test setup of leaf spring landing gear.

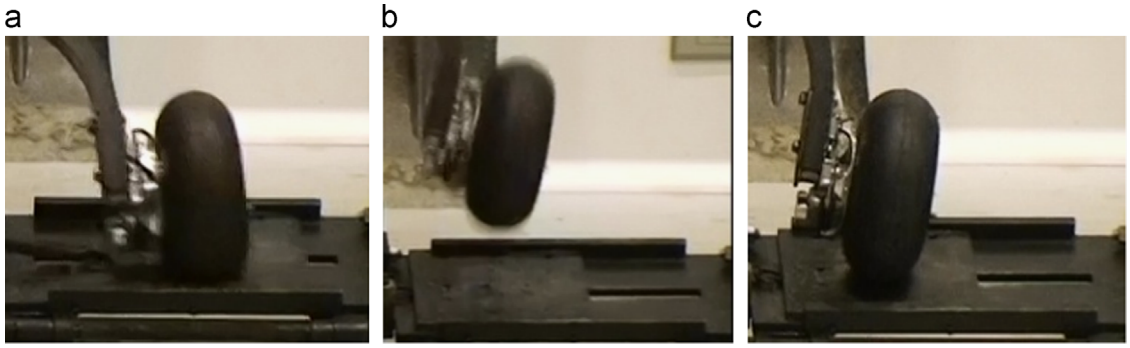

Fig. 12. Drop test – frames of video. (a) Fully compressed, (b) maximum rebound, and (c) stationary state.

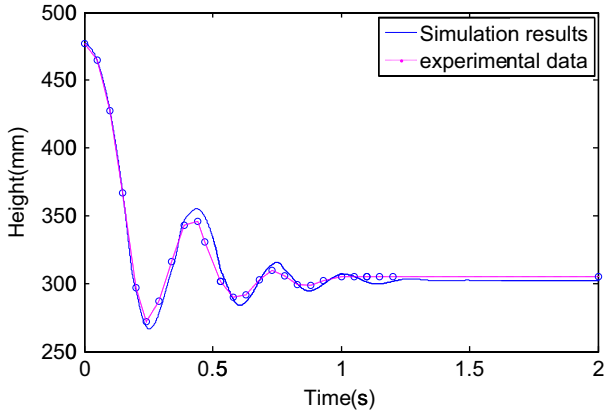

Fig. 13. Height magnitudes of the CG of leaf spring during drop process.

drop test and the warping-multibody simulation is almost indistinguishable on the volume. While a considerable large volume error can be observed from the linear-multibody simulation at the first fully compressed time. The linear-multibody and warped-multibody approach still yield stable simulation even for a time step of 3 ms.

In summary, both the cantilever beam example and leaf spring statics experiments show that the modal warping method has higher accuracy of calculation than linear modal method for large relative rotational deformations. Then the drop simulation/experimental comparison proves the accuracy of the warping-multibody model and a high-speed multibody dynamic analysis is realized.

6. Conclusions

A general and systematic methodology has been presented to integrate the modal warping method into FFRF for modeling leaf spring landing gear. The proposed analysis method is an approximated solution; therefore, it is important to evaluate the degree of error. Both of the accuracy of modal warping method and warping-multibody method are examined by simulation/experimental comparison. Linear modal method, however, fails to capture accurate deformations as the result of the limitation of linear approximation, while the FEM leads to a large number of discretized DOFs in order to achieve accurate solutions. Then the performance of simplified warping-multibody formulation that combines modal warping formula with rigid body simulation was investigated. Based on the results of this study, the following main conclusions can be drawn:

- One of the key properties of the modal warping method is that all expensive computations for matrix are precomputed. Therefore the modal warping method maintains as much of the computation efficient as possible. Meanwhile a good agreement (errors less than 10%) can be observed between the results of the modal warping method and nonlinear FEM.
- The accuracy of the linear modal method is almost same with the modal warping method for small deformations. We also conducted elastic models for some other objects and the performance of the linear modal method is as good as the modal warping method. The exceptions are long, thin, or highly deformable objects. Note that the calculation errors of the both methods increases as the forces/deformations increases.
- The key step of this modeling process consists in reducing the highly number of DOFs to first few modes by a frequency response analysis. 10 modes and 11modes are used respectively to construct the elastic models of cantilever beam and leaf spring landing gear. The accuracy of elastic model does not improve significantly when more modes are used.
- A more accuracy elastic model of leaf spring landing gear can be obtained by using the modes measured from modal experiment to replace the first and/or second mode.
- The drop simulation/experimental errors are introduced both by the modal warping method and by the uncoupling between rigid body motion and deformation. Experimental/simulation comparison proves an acceptable accuracy of the developed model. However, the error of the proposed method may be largely increased when high speed, light weight mechanical systems are considered. Future studies with this model should focus on leaf spring design and UAV model development.

Generally speaking, we observe that the modal warping model is suitable for free floating reference frame formulation to dynamics analysis of cantilever beam type objects especially leaf spring landing gear. It is also effective offering a good potential to be applied to more complex cases such as the ground multibody dynamics analysis of UAV and the gear walk analysis.

Acknowledgments

The project supported by the Knowledge Innovation Program of the Chinese Academy of Sciences (Grant no. YYYJ-1122) and the Innovation Program of UAV funded by the Changchun Institute of Optics, Fine Mechanics and Physics, Chinese Academy of Sciences (CIOMP) (Grant no. 13kz02). We also gratefully acknowledge the support from the Science Fund for Young Scholars of the National Natural Science Foundation of China (Grant no. 51305421).

Appendix A. Supporting information

Supplementary data associated with this article can be found in the online version at http://dx.doi.org/10.1016/j.ijmecsci.2015.01.003.

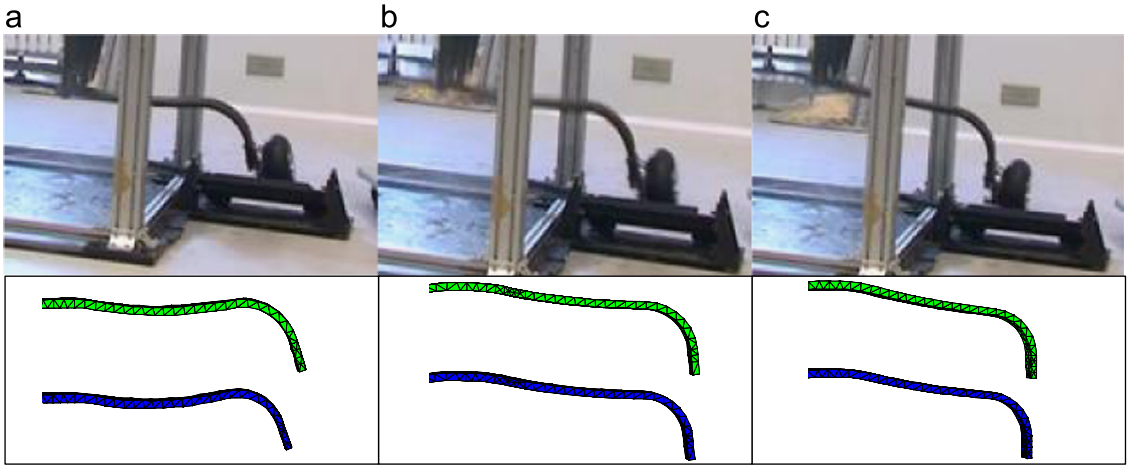

Fig. 14. Fully compressed of the landing gear, drop test, linear-multibody (green), and warping-multibody (blue).

References

[1] Wang HT, Xing JT, Pricea WG, Li WJ. An investigation of an active landing gear system to reduce aircraft vibrations caused by landing impacts and runway excitations. J Sound Vib 2008;317:50–66.
[2] Krüger W, Besselink I, Cowling D. Aircraft landing gear dynamics: simulation and control. Veh Syst Dyn 1997;28(2):119–58.
[3] Kapseong R, A descriptive modeling and simulation of aircraft-runway dynamics, AIAA Paper 2003-1895, 2003.
[4] Collins T, Kochersberger K. Constrained layer damping test results for aircraft landing gear. Struct Dyn 2011;3(12):303–14.
[5] Khapane PD. Gear walk instability studies using flexible multibody dynamics simulation methods in SIMPACK. Aerosp Sci Technol 2006;10:19–25.
[6] Rowland FT. Manual on Design and Application of Leaf Springs. Warrendale, PA: Society of Automotive Engineers (SAE); 1980.
[7] Rill G, Kessing N, Lange O, Meier J Leaf spring modeling for real time applications. In: Proceedings of the dynamics of vehicles on road and on tracks - extensive summaries, IAVSD 03,Atsugi, Kanagawa, Japan 2003.
[8] Zienkiewicz OC. Introductory Lectures on the Finite Element Method. Wien, New York: Springer; 1973.
[9] Li Q, Li W. A contact finite element algorithm for the multileaf spring of vehicle suspension systems. IMECE Part D: J Autom Eng 2004;218:305–14.
[10] Hatch MR. Vibration simulation using MATLAB and ANSYS. Boca Raton, London, NY, Washington, D.C.: Chapman & HALL/CRC; 2000.
[11] Hurty WC. Dynamic analysis of structural systems using component modes. AIAA J 1965;3(4):678–85.
[12] James DL, Pai DK. DyRT: dynamic response textures for real time deformation simulation with graphics hardware department of computer science. ACM Trans Graph 2002;21(3):582–5.
[13] Hauser KK, Shen C, O'Brien JF Interactive deformation using modal analysis with constraints. In: Proceedings of the graphics interface, 2003;247–55.
[14] Mayo JM, Garcia VD, Domfnguez J. Study of the geometric stiffening effect: comparison of different formulations. J Multibody Syst Dyn 2004;11:321–41.
[15] Nickell RE. Nonlinear dynamics by mode superposition. Comput Methods Appl Mech Eng 1976;7:107–29.
[16] Chang CJ, Mohraz B. Modal analysis of nonlinear systems with classical and non-classical damping. Comput Str 1990;36(6):1067–80.
[17] Sugiyama H, Shabana AA, Omar MA, Loh WY. Development of nonlinear elastic leaf spring model for multibody vehicle systems. Comput Methods Appl Mech Eng 2006;195:6925–41.
[18] Wang J, Chen JK, Liao S. An explicit solution of the large deformation of a cantilever beam under point load at the free tip. J Comput Appl Math 2008;212:320–30.
[19] Pai PF, Anderson TJ, Wheater EA. Large-deformation tests and total-Lagrangian finite element analysis of flexible beams. Int J Solids Struct 2000;37:2951–80.
[20] Müller M, Dorsey J, McMillan L, Jagnow R Stable real-time deformations. In: Proceedings of the ACM SIGGRAPH, symposium on computer animation, 2002; 49–54.
[21] Ngan WH, John EL Efficient deformable body simulation using stiffness-warped nonlinear finite elements. In: Proceedings of the interactive 3D graphics and games, 2008.
[22] Shabana AA. Theory of Vibration, Volume II: Discrete and Continuous Systems. NewYork, NY: Springer Verlag; 1990.
[23] Sherif K, Witteveen W, Mayrhofer K. Quasi-static consideration of high-frequency modes for more efficient flexible multibody simulations. Acta Mech 2012;223:1285–305.
[24] Shabana AA. Dynamics of Multibody Systems. UK: Cambridge University Press; 2005.
[25] Neto MA, Ambro´ Sio Jorge AC, Leal RP. Flexible Multibody Systems Models Using Composite Materials Components. Multibody Syst Dyn 2004;12:385–405.
[26] Schwertassek R, Allrapp O, Shabana AA. Flexible multibody simulation and choice of shape functions. Nonlinear Dyn 1999;20:361–80.
[27] Adiprawita W, Ahmad AS, Semibiring J. Hardware in the loop simulator in UAV rapid development life cycle 2008;08:3874.
[28] Jung D, Tsiotras P. Modelling and hardware-in-the-loop simulation for a small unmanned aerial vehicle. AIAA Infotech Aerosp 2007;07:2763.
[29] Monga M, Karkee M, Sun S, Kiran Tondehal L, Steward B, Kelkar A. Real-time simulation of dynamic vehicle models using a high-performance reconfigurable platform. Procedia Comput Sci 2012;9:338–47.
[30] Shiiba T, Obana K, Machida N. Comparison of linearized vs. non-linearized multibody vehicle model for real-time simulation. Int J Non-Linear Mech 2013;53:32–40.
[31] Hoher S, Röck S. A contribution to the real-time simulation of coupled finite element models of machine tools–a numerical comparison. Simul Model Pract Theor 2011;19(7):1627–39.
[32] Choi MG, Ko. HS. Modal warping: real-time simulation of large rotational deformation and manipulation. IEEE Trans Vis Comput Gr 2005;11(1):91–101.
[33] Guo X, Qin H. Real-time meshless deformation. Comput Anim Virt Worlds 2005;16(3-4):189–200.